Renewable Energy 89 (2016) 108–124

Contents lists available at ScienceDirect

Renewable Energy

journal homepage: www.elsevier.com/locate/renene

Optimal flow control of a forced circulation solar water heating system with energy storage units and connecting pipes

Sula Ntsaluba*, Bing Zhu, Xiaohua Xia

Department of Electrical, Electronic and Computer Engineering, University of Pretoria, Pretoria 0002, South Africa

ARTICLE INFO

Article history:
Received 23 June 2015
Received in revised form
8 November 2015
Accepted 17 November 2015
Available online xxx

Keywords:
Flat plate solar collector
Flow rate optimization
Maximum energy extraction
System thermal losses
Thermal comfort

ABSTRACT

This paper focuses on pump flow rate optimization for forced circulation solar water heating systems with pipes. The system consists of: an array of flat plate solar collectors, two storage tanks for the circulation fluid and water, a heat exchanger, two pumps, and connecting pipes. The storage tanks operate in the fully mixed regime to avoid thermal stratification. The pipes are considered as separated components in the system so as to account for their thermal effects. The objective is to determine optimal flow rates in the primary and secondary loops in order to maximize energy transfer to the circulation fluid storage tank, while reaching user defined temperatures in the water storage tank to increase thermal comfort. A model is developed using mainly the first and second laws of thermodynamics. The model is used to maximize the difference between the energy extracted from the solar collector and the combined sum of the energy extracted by the heat exchanger and corresponding energies used by the pumps in the primary and secondary loops. The objective function maximizes the overall system energy gain whilst minimizing the sum of the energy extracted by the heat exchanger and corresponding pump energy in the secondary loop to conserve stored energy and meet the user requirement of water tank temperatures. A case study is shown to illustrate the effects of the model. When compared to other flow control techniques, in particular the most suitable energy efficient control strategy, the results of this study show a 7.82% increase in the amount of energy extracted. The results also show system thermal losses ranging between 5.54% and 7.34% for the different control strategies due to connecting pipe losses.

1. Introduction

Recently, intensive efforts have been made in attempt to either integrate or replace conventional energy sources with renewable energy sources (RES) in order to meet power demands [1]. This is due to the fact that RES are non-polluting and non-depletable whilst they also have low operation and maintenance costs thus making them potential sources of alternative energy [1–3]. Solar water heating systems (SWHS) are among the most common and favourable renewable energy systems as the use of these systems can result in significant energy savings. However, there are limiting factors to be considered when utilizing SWHS. These include:

a) Unpredictable behaviour (energy produced from RES may not always meet the demand)
b) Economic viability
c) Thermal performance

It is therefore essential to investigate ways to overcome these limitations so as to increase the viability of SWHS. A common solution to a) and b) is the use of an effective thermal energy storage system (one that is able to store thermal energy at the highest possible temperature whilst exhibiting minimal thermal losses). The main thermal energy storage techniques include: thermally stratified storage[1] and reversible chemical heat storage.[2] A second method involves integrating SWHS with a flow control device (pump) in order to increase the rate of energy transfer thereby maximizing energy transfer from the solar collector to the energy storage units (tanks) [4,6]. Optimal flow control is therefore an

* Corresponding author.
E-mail address: ntsaluba.sbk@gmail.com (S. Ntsaluba).

http://dx.doi.org/10.1016/j.renene.2015.11.047
0960-1481/

[1] Thermal stratified storage is a technique that is widely used in energy conservation and load management applications. Stratification describes the temperature difference that can exist between different levels inside a tank. A multinode approach (the tank is typically divided into N nodes) is used to characterize the energy in the tank [4,5].

[2] Reversible chemical heat storage is a technique that is based on the conversion of solar radiation into high-temperature heat. This technique utilizes a system of reactants that either transfer energy to the storage tank or extract energy from the tank. The system is connected in an open loop or closed-loop configuration [4].

important factor that can be used to increase the performance of SWHS.

This can be achieved through the application of optimal flow rate strategies. Optimization will however result in different optimal strategies based on the objectives and constraints of the defined problem. For instance, different optimal flow control strategies may be obtained when considering cost minimization as oppose to energy maximization. Existing approaches to energy maximization through mass flow rate control are reported in [4,7–13]. In particular [7], investigates optimal flow control of a closed-loop SWHS with one and two serpentines used for heat exchange in the storage tank. The results show that optimal switching between the minimum and maximum flow rate (mainly known as bang–bang control) yield a greater energy gain, system efficiency and reduced system thermal losses when compared to traditional flow strategies such as constant flow rate, proportional and proportional integral derivative (PID) control. In Ref. [8], optimal operation strategies for SWHS connected in an open loop configuration are considered. The results suggest that a constant optimal mass flow rate (which can be obtained using the overall average of the optimal mass flow rates that are determined for each sample instance of the optimization interval) may be a good strategy during warmer seasons of the year as this can yield results that are very close to the optimum results. In Ref. [10], a low temperature solar water collector connected to a thermally stratified tank is considered with the objective of obtaining optimal mass flow rates required to maximize the net gained energy. The resulting mass flow rate values are close to the minimum and maximum limits which support the strategy of optimal switching between the minimum and maximum available flow rate. In Ref. [9], a co-generation system consisting of a solar collector, gas burner, thermal reservoir, hot water heat exchanger and absorption refrigerator connected in a two loop configuration with two pumps is devised for producing heating as well as cooling. The objective is to maximize the system performance (reduce exergy destruction) whilst also minimizing the system pull up and pull down times (time taken to reach a set point temperature). The results show two optimum constant pump flow rates values for the two pumps. In Ref. [11] an optimal control method for a solar collector loop in a closed-loop configuration is studied. The system is described by a bilinear lumped parameter model for the collector fluid temperature and a bilinear lumped parameter model for the storage fluid temperature. The objective is to obtain optimum values for the collector fluid velocity in order to maximize the net energy that is collected over a fixed time period. The results agree with [8] and [10] in that optimal switching will occur between the minimum and maxim flow limits. The results also show that in instances where only two switches occur during the period of operation, the optimal control is highly dependent on the temperature difference across the collector. In [12,13] the application of block orientated type mathematical modelling is applied to SWHS with pumps. In this paper two different types of bang–bang control are used. In the first type (referred to as ordinary control), the on-off status of the pump is temperature dependent, whilst in the second type (referred to as energy based control) the control action is dependent on the comparison of the available energy to extract and the pump power used to extract this energy. The results show that the energy based control method results in greater energy gain and a higher water tank temperature. In Ref. [14], an energetic optimization of flat plate solar collectors is developed in order to determine the optimal performance and design parameters of the system. The objective is to determine the optimum flow rate and collector aperture area combination that will result in a maximized exergy efficiency. The results illustrate the dependence of exergy on the aperture area and flow rate with maximized exergy outputs correlating to maximum flow rate and aperture area values. Thermal losses due to the pipes connecting the solar collector to the storage unit are assumed to negligible in all the papers discussed above.

In Ref. [15], extended differential equations are used to model a SWHS consisting of a solar collector, heat exchanger, energy storage tank and connecting pipes. The developed model considers pipe thermal losses and simply illustrates the temperature distribution over the components of the SWHS. When compared to measured results from a physical system, the results of this model show lower absolute error than those of other models that do not take system thermal losses into account. The results of Ref. [15] highlight the importance of considering system thermal losses in order to increase the accuracy of any model. In attempt to further the work that has been developed by the previous authors, this paper focusses on flow rate optimization of SWHS with two energy storage tanks and connecting pipes.

There are three novelties to our approach. Firstly, unlike other models that either aim to maximize the energy extracted from the solar collector or to maximize the difference between the energy collected and the energy used by the pumps, our model is developed with two objectives; in the primary loop, the flow rates are optimized for maximum energy transfer to the energy storage tank, whilst in the secondary loop, the flow rates are optimized for minimum energy extraction from the first energy storage tank to the water tank in order to conserve energy whilst meeting user requirement of water tank temperatures at different hours of the day so as to increase thermal comfort. Our objective function therefore aims to maximize the overall energy gain of the SWHS whilst taking into account the energy extracted from the solar collector, the energy used by the pumps as well as the energy transfer that occurs between the two tanks. Secondly, most existing models have optimized flow rates for the daytime period where there is an opportunity to extract energy. Due to the presence of the two energy storage tanks, our model aims to optimize the flow rates of two pumps over a 24 h period as oppose to only during the period when energy available from the collector. Lastly, our SWHS model takes into account pipe thermal losses as well as resulting power losses. Previous optimal flow control models for SWHS do not take these losses into account. In this model, the losses are characterized as a function of the pipe parameters (heat loss coefficients of the pipes) which are calculated for every sample instant as oppose assuming them to be constant, as well as dimensions of the connecting pipe (inner diameter, length, and surface area). This will result in a more realistic model of SWHS that produces optimized flow results that can resemble those of a physical SWHS to a greater degree than current existing models. the developed model aims to optimize the flow rates in the primary and secondary loops whilst meeting user defined water tank temperatures at different hours of the day so as to increase thermal comfort.

The layout of this paper is as follows: The problem formulation is discussed in Section 2. The formulation of the mathematical model is presented in Section 3. The model optimization procedure is presented in Section 4. In Section 5, a case study is presented together with a discussion and analysis of the corresponding results. This study is concluded in Section 6.

2. Problem formulation

The system considered in this paper is shown in Fig. 1. It consists of a flat plate solar collector with surface area A_{coll}, a storage tank (T_1) used to store circulation fluid with mass M_{cf}, and specific heat capacity C_{cf}, a storage tank (T_2) with water tank used to store water with mass M_w, and specific heat capacity C_w, connecting pipes cp_i of

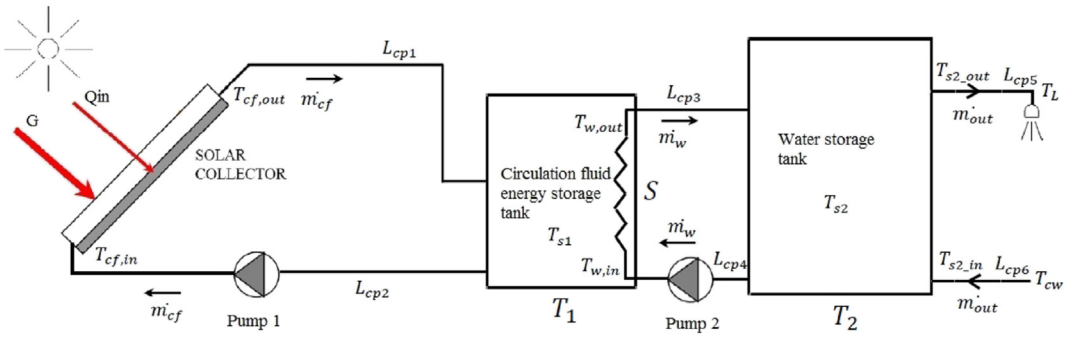

Fig. 1. Forced circulation SWHS to be optimized.

lengths Lcp_i and inner diameter d_{cpi} for $i = 1,\ldots,6$, as well as two pumps used in the primary and secondary loops of the system. In the primary loop, the circulation fluid flowing at a mass flow rate of $\dot{m}_{cf}$ leaves tank T_1 at a temperature of T_{s1}, enters the solar collector at temperature $T_{cf,in}$ and leaves at temperature $T_{cf,out}$. The secondary loop is used to extract energy from tank T_1 through the use of a serpentine (S) with a heat transfer surface area, transfer coefficient and efficiency of A_s, H_s and η_s. In the secondary loop, water flowing at a mass flow rate of $\dot{m}_w$ leaves tank T_2 at temperature T_{s2}, enters the serpentine S at temperature $T_{w,in}$ and leaves the serpentine at a temperature of $T_{w,out}$. In order to ensure that water in tank T_2 is maintained at a certain level, cold water at a temperature of T_c enters tank T_2 at the same mass flow rate $\dot{m}_{out}$ that water is extracted from T_2 for hot water usage. Therefore the secondary part of the system is connected in an open loop configuration.

In tank T_1, a circulation fluid with low specific heat capacity and low freezing point (when compared to water) is selected to ensure that the liquid does not freeze in areas with cold climates. Another benefit of this liquid is that it has a greater capacity to heat up with a smaller change in energy when compared to specific heating capacity of water, thereby increasing the SWHS's capacity to store energy [16].

It should be noted that SWHS configurations similar to that shown in Fig. 1 have been considered in other studies. More notably, similar systems where considered in [9,12,13,15]. What physically differentiates our system from the studies noted above is the circulation fluid and the type of exchanger used the systems primary loop. When considering the mathematical modelling and optimization of this system, none of the studies indicated above model the connecting pipe thermal losses. Finally, the objectives formulated for the system's primary and secondary loop result in a unique problem.

3. SWHS mathematical model

3.1. Connecting pipe loss factors

Any pipe with a surface that is hotter than the surroundings will experience heat as well as energy losses. These losses are affected by a number of factors, with the dominant ones being: the type of material that the pipe is made of as well as the size and surface temperature of the pipe. Pipe insulation is a popular method used to improve the thermal performance of a pipe. It is therefore necessary to model insulation on a pipe in order evaluate a pipes thermal performance [17]. The pipe thermal loss and decrease in temperature are characterized using equations from [5,17–19]. Fig. 2 shows the cross section and length of an insulated pipe.

The thermal loss of the pipe may be obtained using the following relation.

$$Q_{pipe} = L \cdot \pi \cdot D_3 \cdot U_p \cdot (T_{in} - T_a), \tag{1}$$

where: L is the length of the pipe, D_3 the outer diameter, U_p is the pipes overall heat loss coefficient, T_{in} is the pipes inner temperature and T_a is the ambient temperature [17,19]. The decrease in temperature due to the heat losses is approximated by

$$\Delta T_{in} = \frac{U_p \cdot L \cdot \pi \cdot D_3 \cdot (T_{in} - T_a)}{m_p \cdot C_p}, \tag{2}$$

where $\dot{m}_p$ and C_p are the mass flow rate and the specific heat capacity of the fluid flowing in the pipe [5]. The pipes overall heat loss coefficient is determined using the following relation:

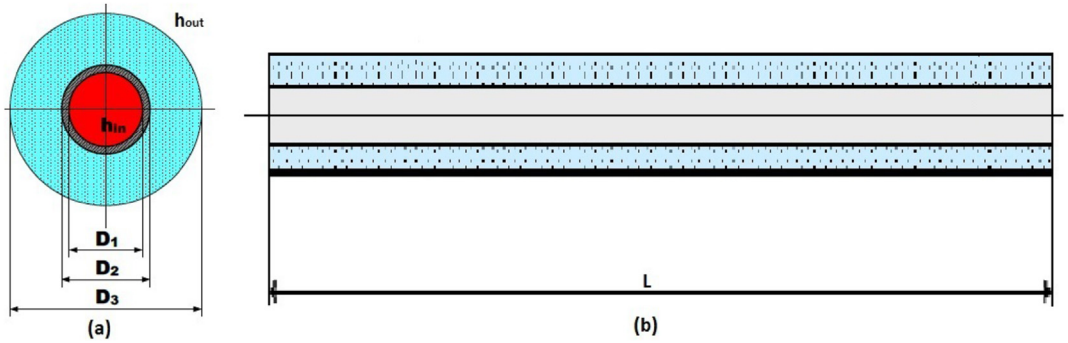

Fig. 2. Connecting pipes of a SWHS. (a) Cross section and (b) Length of the insulated pipe (adapted from [17]).

$$U_p = \left(\frac{1}{\frac{D_3}{D_1 \cdot h_{in}} + \frac{D_3 \cdot \ln\left(\frac{D_2}{D_1}\right)}{2 \cdot k_{pipe}} + \frac{D_3 \cdot \ln\left(\frac{D_3}{D_2}\right)}{2 \cdot k_{insulation}} + \frac{1}{h_{out}}} \right), \quad (3)$$

where D_1, D_2 and D_3 are the pipe insulation diameters as shown in Fig. 2, k_{pipe} and $k_{insulation}$ are the thermal conductivity of the pipe and insulation material, h_{in}, and h_{out} are the heat transfer coefficients of the inner and outer surface of the pipe [17].

3.2. Solar collector

The basic method of measuring the performance of a solar collector is through exposing it to solar radiation and measuring the inlet and outlet temperatures as well as the flow rate of the fluid [5]. The useful heat gain obtained by the circulation fluid is then:

$$Q_{in} = \dot{m}_{cf} \cdot C_{cf} \left(T_{cf,out} - T_{cf,in} \right). \quad (4)$$

In order to determine the useful gain of the flat plate collector, it needs to be characterized such that there is an indication of how it absorbs energy, as well as how it losses energy to the surroundings. The thermal performance of a collector under steady state operating conditions (also known as the useful gain) is given by:

$$Q_{in} = A_{coll} \cdot F_r \left((t\alpha)G - U_L \left(T_{cf,out} - T_{cf,in} \right) \right). \quad (5)$$

This equation is known as the Bliss–Hottel–Whillier relationship where: F_r is the collector heat removal factor, t and α are the transmittance and absorbance factors, G is the global irradiance incident on the aperture plane of the solar collector and U_L is the collector overall heat loss coefficient. The relation used to characterize the collector heat removal factor is:

$$F_r = \frac{\dot{m}_{cf} \cdot c_{cf}}{A_{coll} \cdot U_L} \left[1 - exp\left(\frac{A_{coll} \cdot U_L \cdot F_{prime}}{m_{cf} \cdot c_{cf}} \right) \right], \quad (6)$$

where F_{prime} is denoted as the collector efficiency. All other parameters in eq. (6) are described in Section 2. The overall thermal loss coefficient over the collector is given by:

$$U_L = U_t + U_b + U_e, \quad (7)$$

where: U_t is the collector top thermal loss coefficient, U_b is the collector bottom thermal loss coefficient, and U_e is the collector edge thermal loss coefficients. Physically, these parameters account for the thermal losses experienced in the top, bottom and edges of the solar collector. The overall transmittance and absorbance factors of the solar collector are given by:

$$\tau = \tau_a \cdot \tau_{rn}, \quad (8)$$

$$\alpha = 1 - \tau_a, \quad (9)$$

where τ_a and τ_{rn} denote the collector transmittances due to absorption and reflectance. Equations obtained from [5,20–24] are used to develop a model that characterizes F_{prime}, U_t, U_b, U_e, τ_a and τ_{rn} as functions of the solar collector design parameters in order to determine F_r, t, α, and U_L. This is shown in Appendix A. Further, it is assumed that the useful gain at the collector is the same as the gain available to the circulation fluid.

3.3. Circulation fluid storage tank

In order to characterize the thermal performance of the circulation fluid storage tank, the first law of thermodynamics is applied to it. The energy balance in the tank is then given by the following relation:

$$M_{cf} \cdot C_{cf} \cdot \frac{dT_{s1}}{dt} = Q_{in} - Q_{out\_1} - Q_{loss} - Q_{pipe\_1} - Q_{pipe\_2}, \quad (10)$$

where: M_{cf} is the total mass of the circulation fluid, Q_{out_1} is the heat extracted from tank T_1 in order to heat up water in tank T_2, Q_{loss} is the heat lost in tank T_1 due to the tank thermal properties and Q_{pipe_1}, Q_{pipe_2} are the heat losses due to the connecting pipes in the primary loop [5,7]. This is shown in the Fig. 3.

Q_{loss} is given by the following relation:

$$Q_{loss} = U_{T_1} \cdot A_{T_1} (T_s - T_{int}), \quad (11)$$

where: U_{T1} is the heat transfer coefficient between the circulation fluid stored in tank T_1 and the area that tank 1 is located, A_{T1} is the surface area tank T_1, and T_{int} is the temperature of the area where the storage tank is located [5,7]. Eq. (10) must be integrated over time to determine the long term thermal performance of the storage tank. There are many possible numerical integration methods that can be used to achieve this. In this paper we have used the Runge–Kutta fourth order numerical approximation method (RK4). This method is selected due to the small truncation error per step size associated with it when compared to other methods [25,26].

3.4. Water storage tank

The first law of thermodynamics is applied to water tank (T_2) to form the following relation for the energy balance in the tank:

$$(M_w \cdot C_w) \cdot \frac{dT_{s2}}{dt} = Q_{in\_2} - Q_{load} - Q_{loss\_T2} - Q_{c_w} - Q_{pipe\_3} - Q_{pipe\_4}, \quad (12)$$

where

$$Q_{c_w} = \dot{m}_{out} \cdot C_w (T_{s2} - T_{c_w}), \quad (13)$$

$$Q_{load} = \dot{m}_{out} \cdot C_w (T_{s2} - T_{out}), \quad (14)$$

$$Q_{loss\_T2} = U_{T_{s2}} \cdot A_{T_2} (T_{s2} - T_{int}). \quad (15)$$

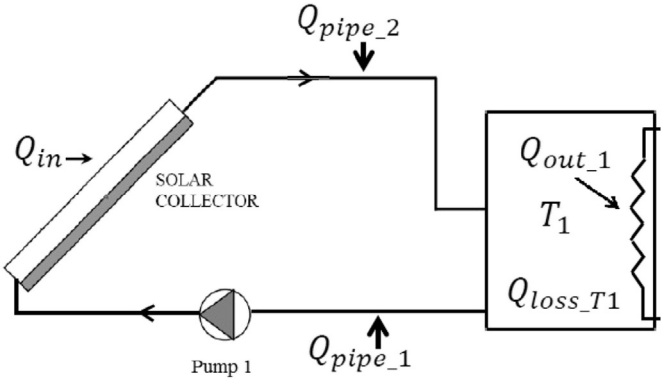

Fig. 3. Rate of energy extraction in the primary loop.

In (13), (14) and (15), M_w and C_w represent the mass and specific heat capacity of water, Q_{in_2} is the heat added to tank T_2 by the heat exchanger in tank T_1, Q_{load} is the heat removed from the tank to the load, Q_{loss_T2} is the thermal losses of the water storage tank, U_{Ts2} is the heat transfer coefficient between the water stored in tank T_2 and the area that tank 2 is located, A_{T2} is the surface area tank T_2, Q_{cw} is the heat removed from the tank through the addition of cold water at a flow rate of $\dot{m}_{out}$, T_{out} is user required value of the temperature at the output of the SWHS and Q_{pipe_3}, Q_{pipe_4} are the heat losses due to connecting pipes cp_i for $i = 3,\ldots,6$. This is shown in Fig. 4.

3.5. Heat exchanger

The heat or rate of energy transfer to the secondary circuit (denoted as Q_{out_1}) is obtained through using a simple model that characterizes the thermal properties of a serpentine which acts as the heat exchanger. In order to further simplify this model, it is assumed that for a short time interval, the temperature (T_{s2}) in the water storage tank (T_2) remains constant. When dealing with a large mass of water (M_w), this assumption is seen to be reasonable as the large mass would result in a small change in (T_{s2}) over a small period of time. Under the above mentioned assumption, the following relations are used to determine the thermal performance of the serpentine:

$$T_{w,out} = T_{s1} + (T_{w,in} - T_{s1})\exp\left(\frac{-h\cdot S}{\eta\cdot\dot{m}_w}\cdot C_w\right), \tag{16}$$

$$Q_{out\_serp} = \dot{m}_w\cdot C_w\left(1-\exp\left(\frac{-h\cdot S}{\eta\cdot\dot{m}_w}\cdot C_w\right)\right)\cdot(T_{s1}-(T_{w,in})), \tag{17}$$

where

$$T_{w,in} = T_{s2} - \Delta T_{in\_pipe\_4}. \tag{18}$$

In (16) and (17), h, η and S denote the heat transfer coefficient, the heat transfer surface area, and the heat transfer efficiency of the serpentine. The heat transfer coefficient is determined using the following relation [7]:

$$h = \frac{h_{lin}}{\pi\cdot D_{serp}}, \tag{19}$$

where h_{lin} and D_{serp} are denoted as the average linear heat transfer coefficient and the diameter of the serpentine. The heat transfer surface area is given by:

$$S = \pi\cdot D_{serp}\cdot L_{serp}, \tag{20}$$

where D_{serp} and L_{serp} are the inner diameter and length of the serpentine. Parameters η is dependent on the type of serpentine selected. Equations obtained from [7,27,28] are used to develop a model that characterizes h and S as functions of the serpentine design parameters. This is shown in Appendix B.

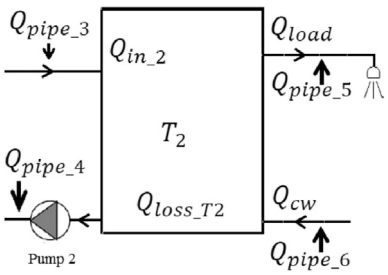

Fig. 4. Rate of energy extraction the secondary loop.

3.6. Flow control

The thermal performance of a solar collector depends on a number of parameters as illustrated in Section 3.2. The main parameters of interest are the mass flow rates ($\dot{m}_{cf}$ and $\dot{m}_w$) which are controlled through the use of a water pump for each of the two fluid circulation loops. The computation of the pump mechanical power required to circulate the fluid in the primary and secondary loops of the system is determined using equations from [7,29]. The pump mechanical power is given by the following relation:

$$P_{pump} = P_{pump,A} + P_{pump,duct}, \tag{21}$$

where: $P_{pump,A}$ represents the power required to cover the pressure losses in the solar collector, and $P_{pump,duct}$ represents the power required to cover the pressure losses in the pipes connecting the solar collector to tank 1 in the primary loop, and connecting tank 1 to tank 2 in the secondary loop. $P_{pump,A}$ is determined using the following equation:

$$P_{pump,A} = \frac{A}{A_{coll}}P_{pump,coll}, \tag{22}$$

where: A represents the surface area of the tubes in the solar collector and $P_{pump,coll}$ represents the energy required to overcome the pressure losses ΔP_{coll} in a single collector. the equations for these parameters are shown below:

$$P_{pump,coll} = \frac{\dot{m}_{coll}}{\rho_{cf}}\Delta P_{coll}, \tag{23}$$

$$\Delta P_{coll} = \zeta_{coll}\frac{\rho_{cf}\cdot w_{coll}^2}{2}, \tag{24}$$

where

$$w_{coll} = \frac{\dot{m}_{coll}}{\rho_{cf}\cdot a_{coll}}. \tag{25}$$

Parameters w_{coll}, ρ_{cf}, ζ_{coll} and a_{coll} represent the fluid speed at the inlet of the collector, the working fluid mass density, the pressure loss coefficient and the cross sectional surface area at the collector's inlet. The mass flow rate at the input of the collector is given by:

$$\dot{m}_{coll} = \frac{A_{coll}}{A}\dot{m}_{cf}. \tag{26}$$

Combining (22)–(26) results in the following relation:

$$P_{pump,A} = K_{pump,A}\cdot\dot{m}_{cf}^3, \tag{27}$$

where the coefficient $K_{pump,A}$ is determined using:

$$K_{pump,A} = \frac{\zeta_{coll}}{2\rho_{cf}^2}\left[\frac{A_{coll}}{a_{coll}\cdot A}\right]^2. \tag{28}$$

The pump power necessary to cover the pressure losses over the collector ducts in the (SWHS) is given by:

$$P_{pump,duct} = \frac{\dot{m}_{cf}}{\rho_{cf}} \Delta P_{duct}, \tag{29}$$

where $\dot{m}_{cf}$ and ρ_{cf} represent the fluid speed in the ducts and the working fluid mass density. ΔP_{duct} represents the pressure losses over the ducts and is given by:

$$\Delta P_{duct} = \lambda_{duct} \frac{l_{duct}}{d_{duct}} \cdot \frac{\rho_{cf} \cdot w_{duct}^2}{2}, \tag{30}$$

where λ_{duct}, l_{duct} and d_{duct} are the friction factor of the duct, the length of the duct and the inner diameter of the duct. The fluid speed in the duct (w_{duct}) is given by:

$$w_{duct} = \frac{4}{\pi} \frac{\dot{m}_{cf}}{\rho_{cf} \cdot d_{duct}^2}. \tag{31}$$

Combining (29)–(31) yields:

$$P_{pump,duct} = K_{pump,duct} \cdot \dot{m}_{cf}^3, \tag{32}$$

where the coefficient $K_{pump,duct}$ is given by:

$$K_{pump,duct} = \frac{8}{\pi^2} \frac{\lambda_{duct} \cdot l_{duct}}{\rho_{cf}^2 \cdot d_{duct}^5}, \tag{33}$$

Finally, combining (27), (28), (32) and (33) yields:

$$P_{pump} = K_{pump} \cdot \dot{m}_c f^3 \tag{34}$$

where

$$K_{pump} = K_{pump,A} + K_{pump,duct}. \tag{35}$$

The rate of energy usage of pumps P_1 and P_2 can therefore be individually denoted as follows:

$$P_{pump_1} = K_{pump_1} \cdot \left(\dot{m}_{cf}\right)^3, \tag{36}$$

$$P_{pump_2} = K_{pump_2} \cdot (\dot{m}_w)^3. \tag{37}$$

It should be noted that for P_2, $K_{pump,A} = 0$ as there is no solar collector connected in the secondary loop. Using equations obtained from [7,30,29], ζ_{coll} and λ_{duct} are characterized as functions of the pump design parameters. This is shown in Appendix C.

4. Model optimization

In order to develop a model that will maximize the energy gain in the primary loop whilst minimizing energy usage by the pumps as well as the rate of energy extraction from tank 1 to meet the energy requirements of tank 2 in the secondary loop, the following continuous time objective function is formulated:

$$J\left(\dot{m}_{cf}, \dot{m}_w\right) = \int_{t=0}^{T} \left[Q_{in}\left(\dot{m}_{cf}\right) - \left(P_{pump1}\left(\dot{m}_{cf}\right) + P_{pump2}(\dot{m}_w)\right)\right] dt. \tag{38}$$

where T denotes the terminal time or optimization interval which is selected as 24 h. The objective function is then expressed in the discrete time domain. This is given by:

$$J\left(\dot{m}_{cf}(i), \dot{m}_w(i)\right) = \sum_{i=1}^{N} \Big[\Big(Q_{in}\left(\dot{m}_{cf}(i)\right) - \Big(P_{pump1}\left(\dot{m}_{cf}(i)\right) + P_{pump2}(\dot{m}_w(i))\Big)\Big) \cdot \Delta_i\Big], \tag{39}$$

where:

$$N = \frac{T}{h}. \tag{40}$$

The sample interval which is denoted as h is chosen as 10 min. Our objective is to maximize this discrete energy function which consists of the rate of energy transfer over the collector (Q_{in}) and the power of the pumps in the primary and secondary loops (P_{pump1} and P_{pump2}). We therefore aim to maximize the difference between the gain over the SC and the energy used by the pumps and in doing so, to maximize the overall gain of the SWHS. This is achieved through negating and minimizing (39) as this is equivalent to maximizing the original function. This is done in order to meet the structural requirements of the Matlab toolbox used to solve the model. The optimization process is then summarized as follows:

$$min\Big[-J\left(\dot{m}_{cf}(i), \dot{m}_w(i)\right)\Big], \tag{41}$$

subject to the following linear inequality constraints:

$$\dot{m}_{cf}^{min} \le \dot{m}_{cf}(i) \le \dot{m}_{cf}^{max}, \tag{42}$$

$$\dot{m}_w^{min} \le \dot{m}_w(i) \le \dot{m}_w^{max}, \tag{43}$$

$$T_{s1}^{min} \le T_{s1}(i) \le T_{s1}^{max}, \tag{44}$$

$$T_{s2}^{min} \le T_{s2}(i) \le T_{s2}^{max}, \tag{45}$$

for $i = 1,\ldots,N$, the following linear equality constraints:

$$T_{cf,in}(i) = T_{s1}(i) - \Delta T_{in,pipe\_2}(i), \tag{46}$$

$$T_{s1}(i) = T_{cf,out}(i) - \Delta T_{in,pipe\_1}(i), \tag{47}$$

$$T_{s2}(i) = T_{w,out}(i) - \Delta T_{in,pipe\_3}(i), \tag{48}$$

$$T_{w,in}(i) = T_{s2}(i) - \Delta T_{in,pipe\_4}(i), \tag{49}$$

$$T_{out}(i) = T_{s2}(i) - \Delta T_{in,pipe\_5}(i), \tag{50}$$

$$T_{s2\_in}(i) = T_{cw}(i) - \Delta T_{in,pipe\_6}(i), \tag{51}$$

for $i = 1,\ldots,N$, and the following non linear inequality constraint:

$$Q_{out\_serp}(i) \ge Q_{in\_2}(i), \tag{52}$$

for $i = 1,\ldots,N$, where: $\dot{m}_{cf}^{min}$, $\dot{m}_{cf}^{max}$, $\dot{m}_w^{min}$ and $\dot{m}_w^{max}$ are the minimum and maximum allowable fluid flow rates for pumps $P1$ and $P2$, while T_{s1}^{min}, T_{s1}^{max}, T_{s2}^{min} and T_{s2}^{max} are the minimum and maximum allowable fluid tank temperatures based on the tank design parameters. Eqs. (46)–(51) regulate the temperature distribution in the SWHS taking into account the temperature losses in the connecting pipes ($\Delta T_{in,pipe\_j}$ where $j = 1,\ldots,6$ according to Fig. 1) for each sample instant over the optimization interval, while (52) ensures that the rate of energy extraction by the serpentine meets the

minimum requirement from tank 2 in order to heat water up to the desired user temperature. It should be noted that (46)–(51) represents system equations that satisfy the system model derived in Section 3.

4.1. Model computational procedure

This section highlights the computational steps of the model. The aim is to obtain optimal flow rates that will maximize the rate of energy extraction from the solar collector in the systems primary loop, whilst minimizing the rate of energy usage of the pumps and the serpentine in the system's secondary loop. With the initial conditions, upper and lower bounds of the control variables ($\dot{m}_{cf}$ and $\dot{m}_w$) set, the optimization command is executed. The command points to an energy function whose input variables are the control variables ($\dot{m}_{cf}$ and $\dot{m}_w$) ranging from 0.00001 to 0.1 kg/s in order to find the optimal solution that will minimize (41) over the 24 h optimization interval. In this function, the secondary loop is analyzed first in order to determine the rate of energy required from T_1 to obtain the required values of T_{out}. In addition to the parameters shown in Tables 2–4, the developed model uses initial values for T_{s1_i}, T_{cw_i}, T_{pm_i} and T_{fm_i} as entry points. With the user requirement of temperature values at the output of the SWHS (T_{out}) known over the 24 h optimization interval, Ts_{2_i} is determined using (50). The rate of energy transfer to the load (Q_{load_i}), the rate of energy loss due to the thermal properties of tank 2 ($Q_{loss\_T2_i}$) and the rate of energy loss (Q_{cw_i}) due to cold water entering tank 2 at temperature T_{s2_i} are calculated using (13), (14) and (15). With $T_{s2_{(i+1)}}$ known, the required rate of energy from the circulation fluid water tank ($Q_{in\_2_i}$) is then calculated using (12). In the system's primary loop, (7)–(9) are used to determine U_L and the transmittance absorbance product ($t\alpha$) for the first sample instance. F_{r_i}, Q_{in_i}, Q_{loss_i}, Q_{out_serpi}, P_{pump1_i}, P_{pump2_i} and $T_{cf.out_i}$ are then calculated. Using these values, the value of $Ts_{(i+1)}$ is calculated using (10). The value of $Ts_{(i+1)}$ is then used to calculate $T_{pm_{(i+1)}}$ and $T_{fm_{(i+1)}}$ using (67) and (78) which can be found in Appendix A. The model therefore simulates this process with flow rates $\dot{m}_{cf}$ and $\dot{m}_w$ ranging from 0.00001 to 0.1 kg/s to find the optimal solution that will minimize (41) over the 24 h optimization interval.

5. Case study

The objective of this case study is to illustrate the effects of mass flow rate optimization on the total energy gain, pipe thermal losses and overall system efficiency of a SWHS. The system to be optimized is a residential forced circulation SWHS that consists of an array of six flat plate solar collectors connected to a circulation fluid storage tank, which in turn is connected to a water tank as shown in Fig. 1.

5.1. Data presentation

Table 1 (values adapted from [5,7,31]) shows the parameters of tank 1 and tank 2 as well as the parameters of the fluids in the tanks.

The system's solar collector parameters are shown in Table 2 (values adapted from [5,7,15]).

The heat exchanger, connecting pipe and primary and secondary loop pump parameters are shown in Table 3 (values adapted from [5,7,17]).

Meteorological obtained from Ref. [12] was used in this study. The measured radiation and ambient temperature (at a constant wind velocity of 3.4 m/s) for 10 min intervals over a 24 h optimization interval are shown in Figs. 5 and 6.

The initial temperature of fluid in storage tank 1 is set at 75 °C to ensure that there is sufficient energy to meet the water heating requirement of tank 2 during the initial optimization period without solar radiation. The required water mass flow rates and water temperature at the output of the SWHS over the 24 h optimization interval is shown in Table 4.

From Table 4, it can be seen that the hot water demand occurs at different periods over the 24 h optimization interval, which presents the opportunity to optimize the mass flow rates in both the primary and the secondary loops of the SWHS during periods where solar radiation is available (daytime), and in the systems secondary loop during periods where there is no available solar radiation (nighttime).

Table 1
Fluid and tank parameters.

Parameter	Symbol	Value	Unit
Tank 1 (*circulation fluid* (*Duratherm* 600))			
Tank diameter	D_{tank_1}	0.69	m
Tank height	H_{tank_1}	1.6	m
Tank volume	V_{tank_1}	598	l
Fluid specific heat capacity	C_{cf}	1967	J (kg K)$^{-1}$
Fluid mass density	ρ_{cf}	844.17	kg m^{-3}
Tank 2 (*water*)			
Tank diameter	D_{tank_2}	0.69	m
Tank height	H_{tank_1}	0.535	m
Tank volume	V_{tank_1}	200	l
Tank specific heat capacity	C_w	4185	J (kg K)$^{-1}$
Tank mass density	ρ_w	1000	kg m^{-3}

5.2. Results and discussion

5.2.1. Primary and secondary loop mass flow rates

Operating the pump at one single speed is a common practice that is applied to such systems, however the system does not operate at its optimal state. In order to illustrate the difference in system performance based on different control strategies, the results of two different strategies are compared to the results obtained using the developed model and the fmincon solver in the MATLAB optimization toolbox [32]. The first control strategy is bang–bang control. This strategy is commonly used in practice with mass flow rate values switching from 0.00001 kg/s (during

Table 2
Flat plate solar collector parameters.

Parameter	Symbol	Value	Unit
Medium 1 (*air*)			
Relative reflective index	n_1	1	–
Medium 2 (*transparent layer*)			
Number of transparent layers (cover)	N	1	–
Thickness of each layer	lt	0.004	m
Relative reflective index	n_2	1.526	–
Emittance	ε_g	0.88	–
Absorption factor/coefficient	k_{abs}	4	m^{-1}
Absorber plate (*aluminium*)			
Emittance	ε_p	0.1	–
Absorbance	α	0.9	–
Thickness	δ_p	0.0015	m
Thermal conductivity	kp	211	W (m K)$^{-1}$
Mass density	ρ_m	2700	kg.m^{-3}
Specific heat capacity	c_m	896	J (kg K)$^{-1}$
Tube external diameter	D_{out}	0.013	M
Tube internal diameter	D_i	0.01	m
Tube length	l_{pipe}	1.5	m
Drum diameter	d_{coll}	0.035	m
Bond conductance	C_b	15	mK W^{-1}
Bottom thermal insulation (*polyurethane*)			
Thickness of the bottom thermal insulation	L_b	0.05	m
Thermal conductivity	k_b	0.034	Wm^{-2} K^{-1}

Table 3
Heat exchanger, connecting pipe and pump parameters.

Parameter	Symbol	Value	Unit
Heat exchanger (*serpentine*):			
Length	L_{serp}	10	m
Inner diameter	D_{serp}	0.025	m
pipe wall thickness	w_{serp}	0.002	m
Heat transfer efficiency	η_0	0.1	–
Surface area	S_0	1.57	m^2
Connecting pipes:			
Pipe inner diameter	D_1	0.0825	m
Pipe inner diameter	D_2	0.0825	m
Pipe outer diameter	D_3	0.189	m
Length of each of the pipes	L_{cp}	5	m
Thermal conductivity of pipe	K_{pipe}	67	W (m K)$^{-1}$
Thermal conductivity of insulating material	K_{ins}	0.07	W (m K)$^{-1}$
Pump 1 *and pump* 2:			
Rated power	p_{pump_r}	53	W
Maximum pump angular velocity	w_a	2430	rpm
Maximum pump linear velocity	w_l	1.2732	m/s

Table 4
Required output water mass flow rate and output temperature.

Time (30 min)	M_{out} (kg s^{-1})	Required T_{s2} (°C)
00:00–03:00	0.00001	41
03:00–03:10	0.1	50
03:10–03:20	0.1	60
03:20–13:00	0.00001	41
13:00–13:10	0.1	50
13:10–20:00	0.00001	41
20:00–20:10	0.1	50
20:10–22:00	0.00001	41
22:00–22:10	0.1	50
22:10–22:20	0.01	45
22:20–24:00	0.00001	41

periods without solar radiation) to 0.1 kg/s (during periods with solar radiation) [7,33]. The second control strategy is adapted from [7]. This strategy is referred to as optimal switching and requires the flow rate to be kept at a minimum during periods where there is little to no available solar radiation. The flow rate then alternates between its minimum and maximum limits during periods where

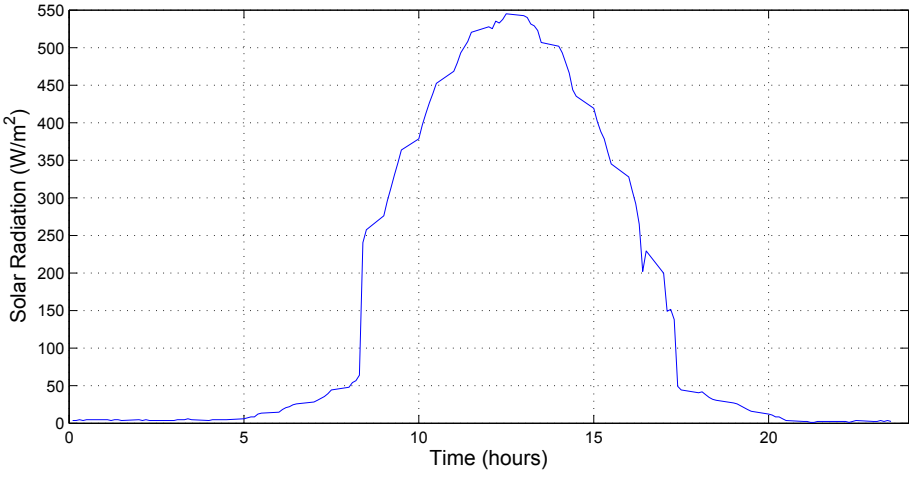

Fig. 5. Solar radiation over the 24 h optimization interval.

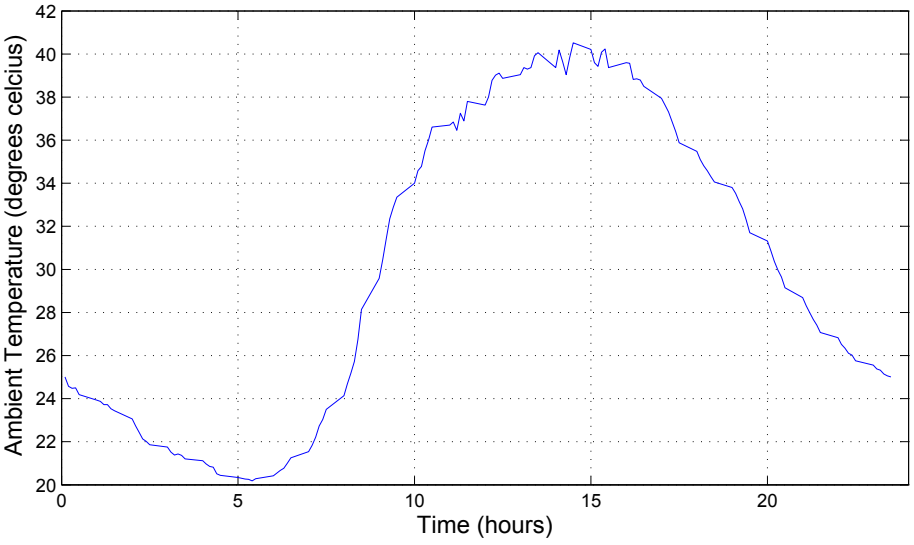

Fig. 6. Ambient temperature.

the energy to be collected exceeds the energy used by the pump. This is done to reduce the system's overall pump power utilized as well as the system thermal losses [7]. This strategy is only applied to the primary loop of the system as the secondary loop is not exposed to solar radiation. Figs. 7 and 8 show the different mass flow rates corresponding to the control strategies discussed above for the primary and secondary loops of the SWHS.

When analyzing Fig. 7, it can be seen that the primary loop average mass flow rates of the optimal solution is less than that of any of the other control strategies. It is expected that the resulting solar collector rate of energy extraction will be less than that of the other two strategies. The pump power used in the primary loop is also expected to be less than that of the other two strategies due to the lower mass flow rates of the optimal solution. In Fig. 8, it can be seen that the secondary loop mass flow rates of the proposed solution are less than those of any of the two strategies. It should be noted that in Fig. 8, the mass flow rates for strategy 1 and 2 are the same. The rate of energy extraction of the heat exchanger for the optimal solution and secondary loop pump power is expected to be less than that of the other two strategies due to the lower mass flow rates of the optimal solution.

5.2.2. Primary and secondary loop pump power

The power utilized by the pumps in the systems primary and secondary loop is shown in Figs. 9 and 10.

From Figs. 9 and 10, it is seen for the proposed solution, the corresponding pump power utilized over the optimization interval is less than that of the other two strategies as was expected. Upon closer inspection of these two figures, it is evident that in the primary loop, the maximum power of the pump is 17.73 W which is 33% of the pump's rated power, whilst in the secondary loop, the maximum power of the pump is 15 W which is 28.3% of the pump's rated power. Though the mass flow rates of the optimal solution result in lower pump power values and an increased system gain, it should be noted that the pumps run at a reduced operational efficiency due to the lower pump power values resulting from the low mass flow rates of the proposed solution. In order to increase the operational efficiency of a pump, the pump must be operated at power values that are close to the rated power of the pump. Therefore, a solution for this would be to reduce the size and rated power of the selected pump.

5.2.3. Rate of energy extraction, gain and thermal losses

The gain of the solar collector is shown in Fig. 11.

When analyzing Fig. 11, it can be seen that for the proposed solution, the gain over the solar collector is less than that of the two other strategies as was expected due to the lower mass flow rates of the optimal solution.

The overall gain of the system is shown in Fig. 12.

The overall gain of the system is characterized as the difference between the gain of the solar collector and power used by the pumps in the primary and secondary loops. From this figure, it can be seen that the different control strategies result in both positive as well as negative power gains over the 24 h interval. The negative gains are attributed to the heating requirement of tank 2 in order to reach the required output temperature T_{out}. Negative gains are obtained when the heating requirement occurs during periods where there is no available solar radiation. From Fig. 12, it can be seen that the mass flow rates of the proposed solution result in the largest gain over the 24 h interval and this is attributed to the following reasons:

a) The pump flow rates are kept to a minimum during periods without solar radiation and with no water heating requirement tank 2.
b) During periods where there is a heating requirement for tank 2 but with no available solar radiation, the secondary loop flow rates are the minimum flow rates required to ensure that the required water heating is achieved.
c) The average pump power of the proposed solution is smaller than any of the other strategies, resulting in smaller pump power usage values and a smaller heat exchanger energy extraction rate when compared to the other strategies.

With smaller pump power usage and heat exchanger energy extraction rate values, the proposed solution results in an overall system gain that is maximized beyond that of the other two control strategies.

When analyzing the rate of energy gain of the heat exchanger, it was found that the optimal solution results in the least amount of

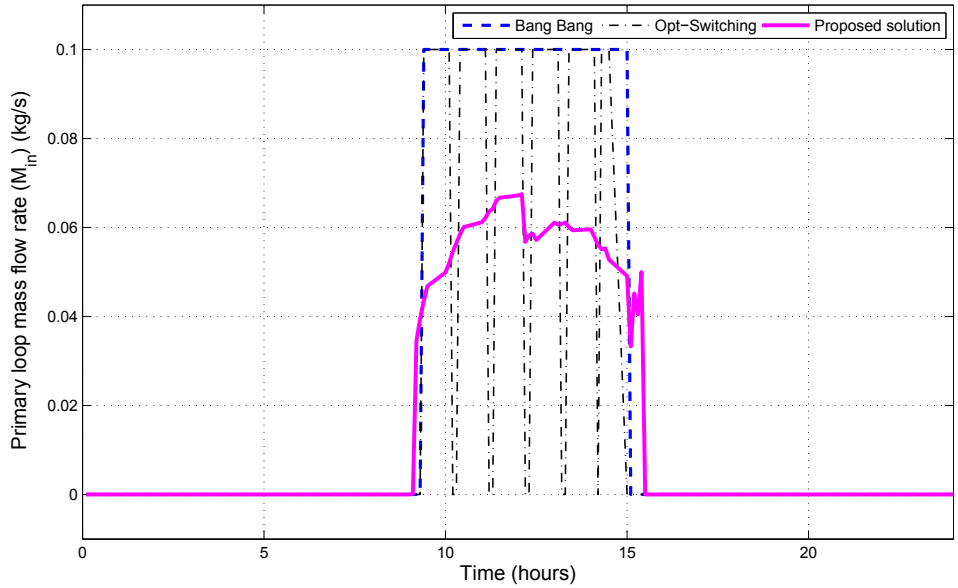

Fig. 7. Primary loop mass flow rates.

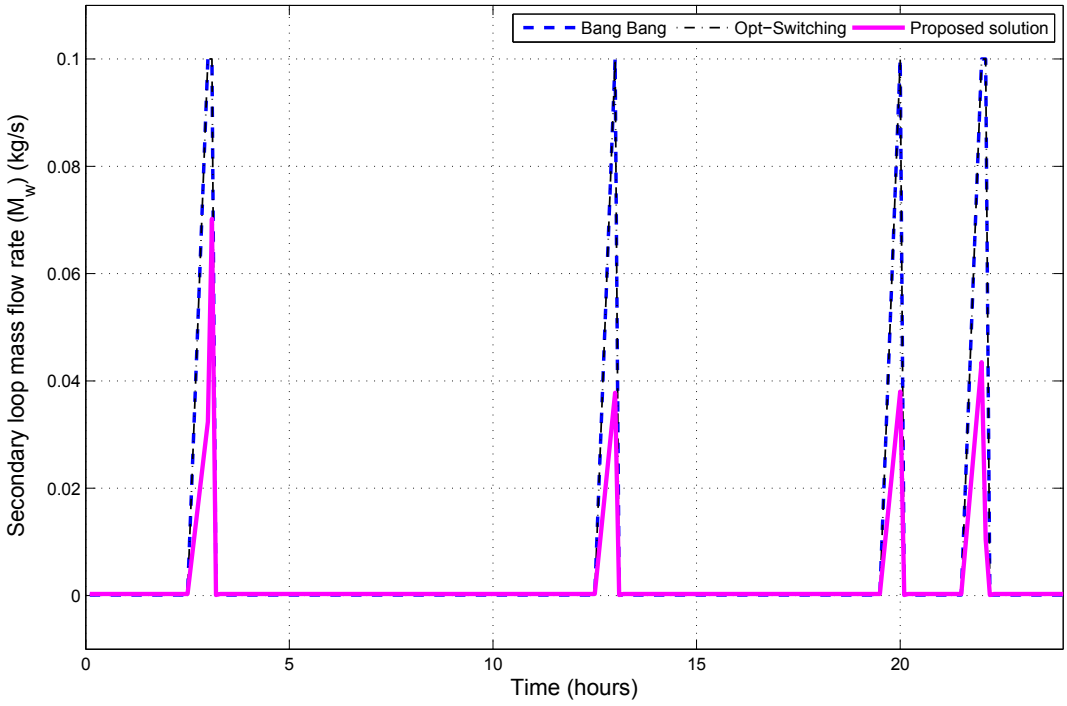

Fig. 8. Secondary loop mass flow rates.

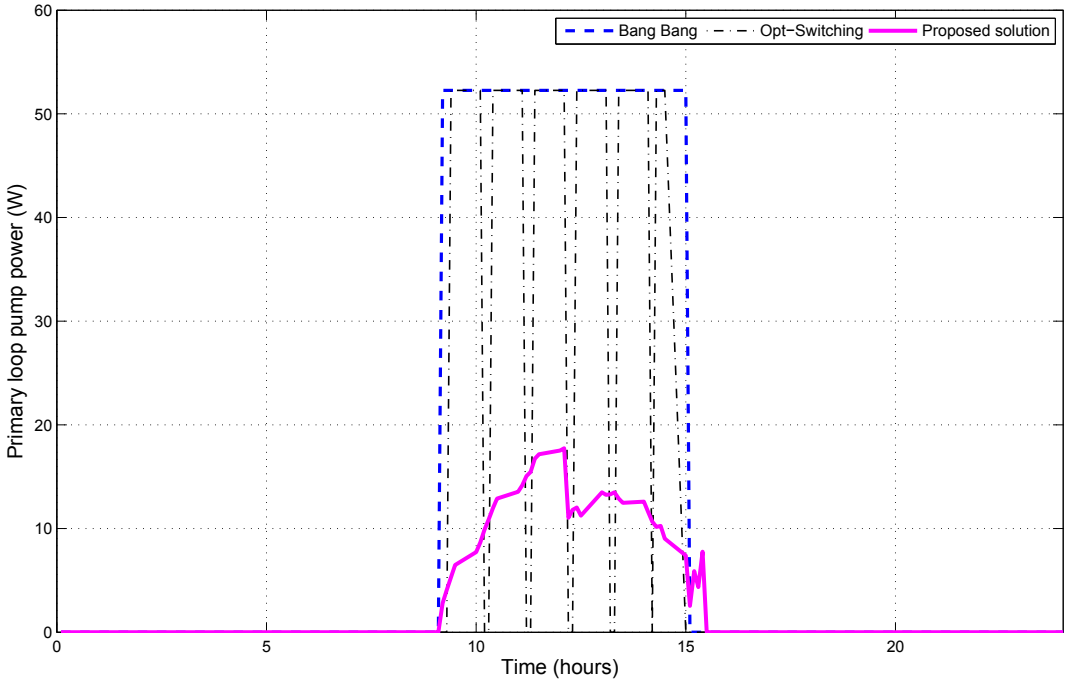

Fig. 9. Primary loop pump power.

energy extracted by the heat exchanger in tank 1 to meet the temperature requirements of tank 2. This is shown in Table 5. The combination of minimum values for heat exchanger energy extraction rate and secondary loop pump usage power ensure that energy in the secondary loop is minimized.

Fig. 13 shows the systems overall accumulative gain.

Since the maximum gain is obtained using the optimal flow rates (Fig. 12), it follows that these flow rates will also produce the highest accumulative energy as can be seen in Fig. 13.

The thermal losses for the two storage tanks is shown in Fig. 14.

From Table 5, it can be seen that the optimal switching control strategy results in the lowest tank thermal losses whilst the bang–bang control strategy results in the highest losses. This is expected as a higher mass flow rates would result in larger tank thermal losses. The alternating action of the optimal switching control strategy results in a reduction in the tank thermal losses

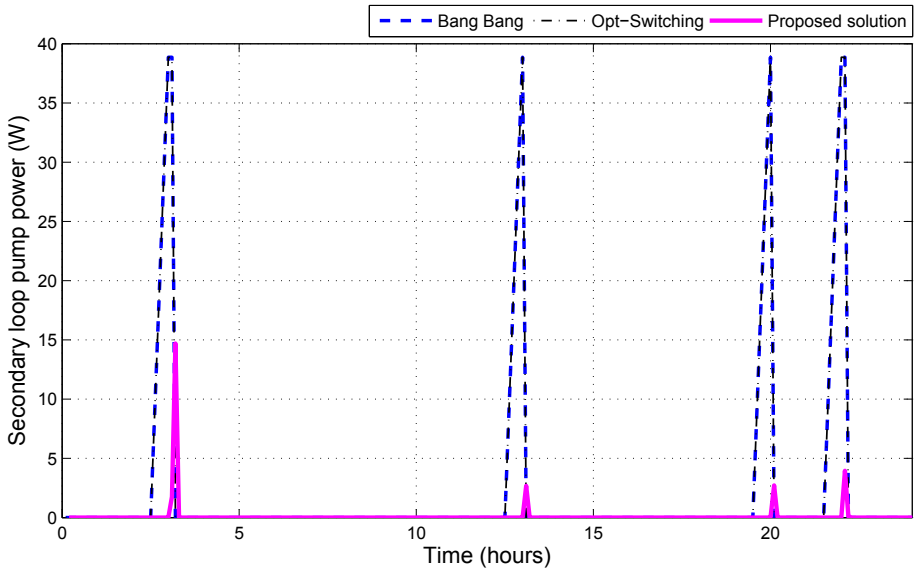

Fig. 10. Secondary loop pump power.

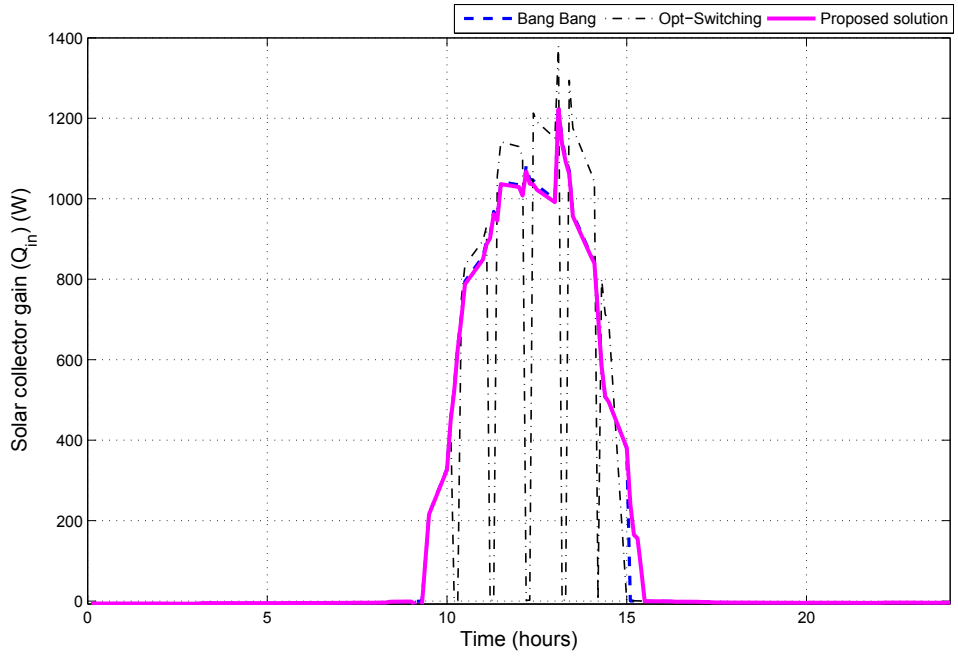

Fig. 11. Solar collector gain.

during instances when the pump is off, thereby reducing the overall thermal losses of the tank. The connecting pipe thermal losses are shown in Fig. 15.

There are a number of factors that contribute to connecting pipe losses. The results of Fig. 14 illustrated the influence that mass flow rates have on thermal losses. It is therefore known that higher losses will be experienced with higher mass flow rates and lower losses with low mass flow rates. In Fig. 15, it can be seen that the connecting pipe thermal losses of the different control strategies are very close, though they do slightly differ as shown in Table 5. The profile has four steep declines that correspond to the periods where energy is being transferred from the primary loop to the secondary loop to meet the water heating requirements. There is a decrease in thermal losses during the early hours of the day. This occurs because the temperature of the primary tank decreases as energy is being transferred from it, resulting in a small difference between the fluid temperature in the connecting pipes from the tank and the ambient temperature, and hence a reduction in the overall tank thermal losses according to (1). It can also be seen that the connecting pipe thermal losses gradually increase during periods where solar radiation is available as during these periods, the primary loop mass flow rates are significantly high, thereby increasing the thermal losses of the connecting pipes. Using (1), the accumulative thermal losses for the bang–bang, optimal switching and proposed solution control strategies are found to be 1.44 KW, 1.38 KW and 1.438 KW respectively. From these values, it can be seen that there is a minimal difference in the pipe thermal losses that can be attributed to the different control strategies.

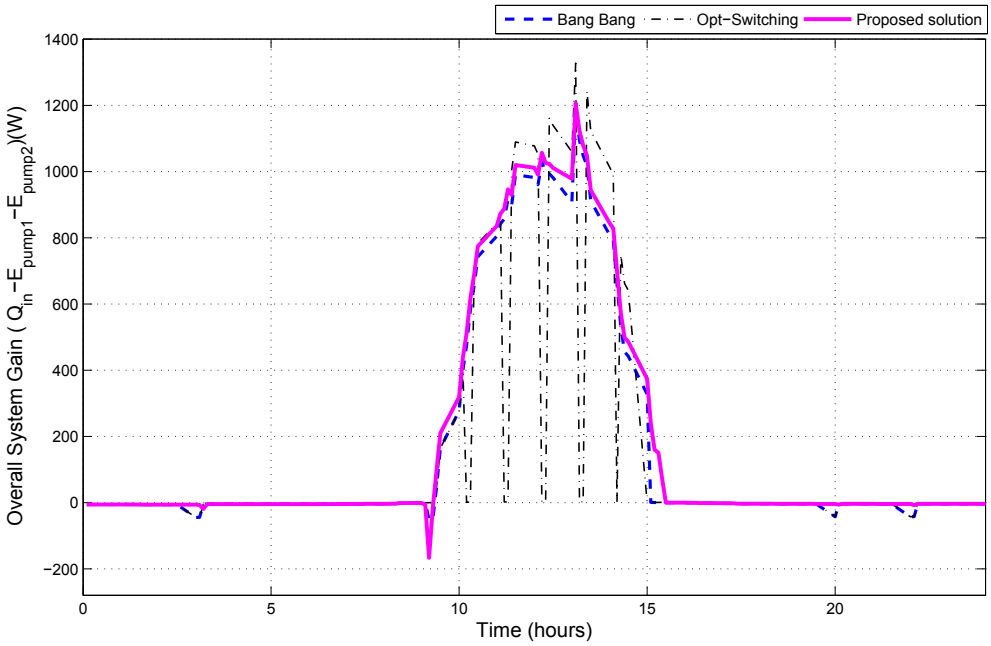

Fig. 12. Overall system gain.

Table 5
Summary of results.

Control strategy	Bang–bang	Opt-switching	Proposed solution
Primary loop pump average power (W)	15.37	8.34	2.95
Secondary loop pump average power (W)	1.62	1.62	0.18
Heat exchanger gain (KW)	88.13	88.13	51.64
Accumulative energy gain (MJ)	14.43	11.31	15.56
Tank thermal losses (KW)	6.89	6.75	6.86
Pipe thermal losses (KW)	1.45	1.38	1.43

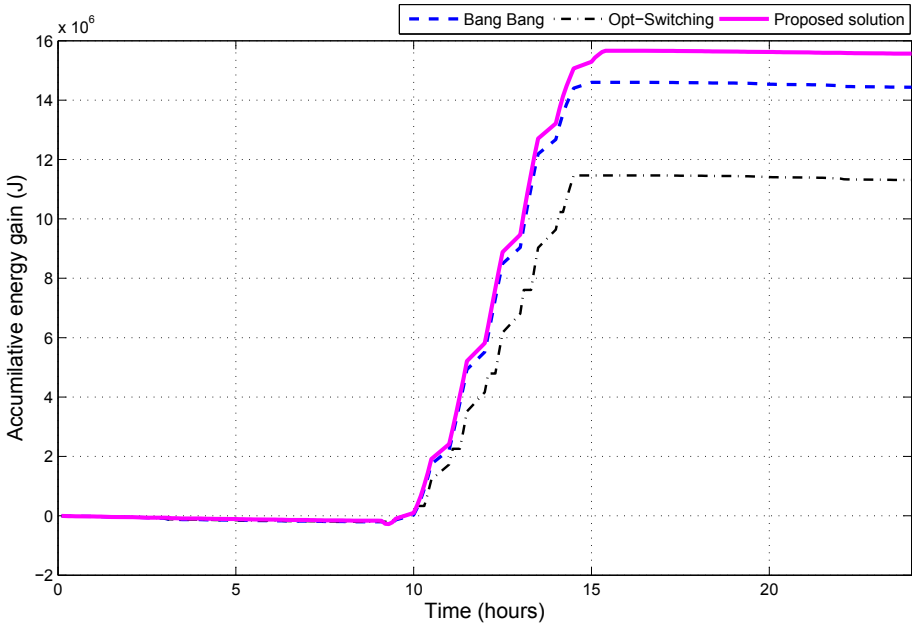

Fig. 13. Accumulative energy gain.

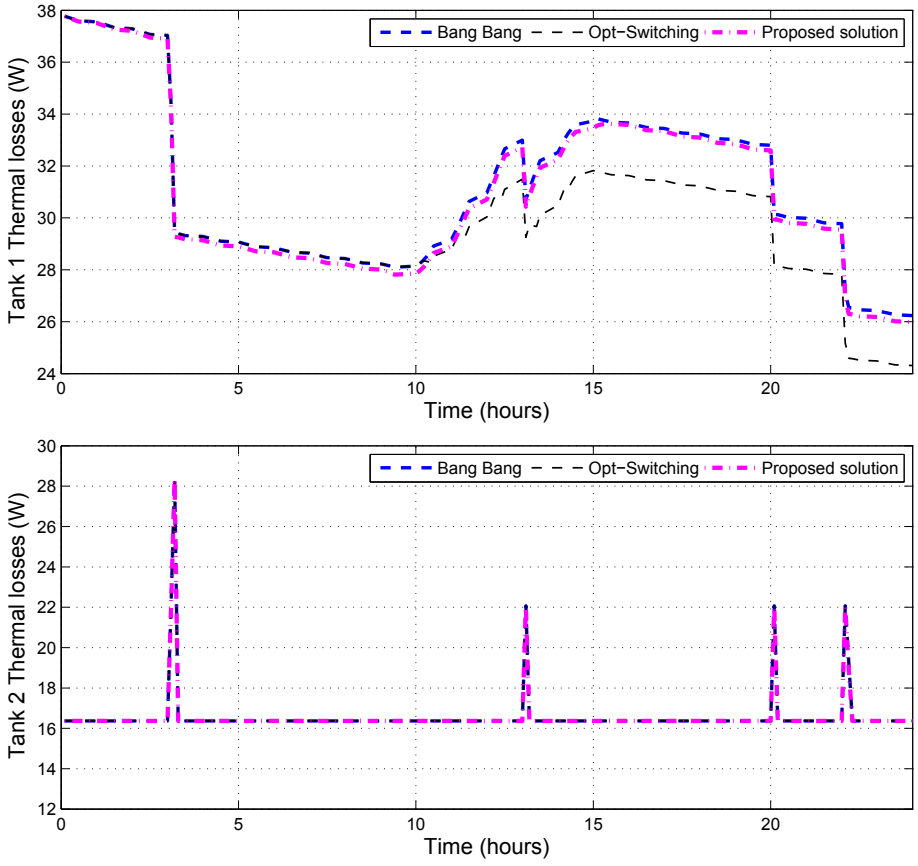

Fig. 14. Thermal losses for tank 1 and tank 2.

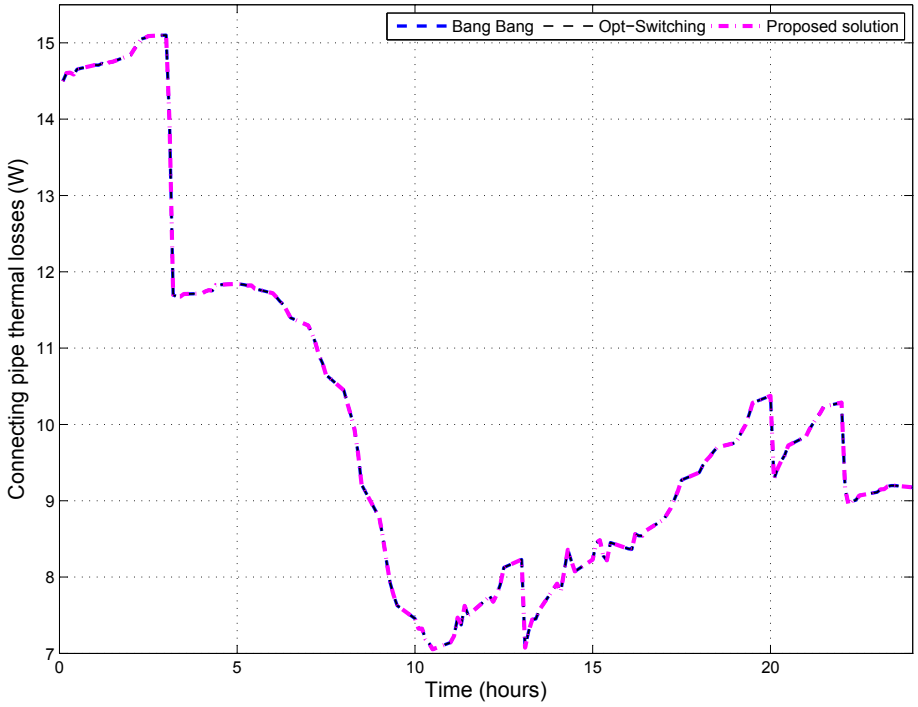

Fig. 15. Connecting pipe thermal losses.

The results of this study are summarized in Table 5.

In this table, the primary and secondary loop average power obtained is the average of (27) and (34) over the optimization interval. The heat exchanger gain and system accumulative energy gain are obtained using (17) and (39) over the optimization interval. The tank and connecting pipe thermal losses are obtained using (1) and (11) over the optimization interval. The system gain is obtained can be seen that the proposed solution results in the lowest average pump power in the primary and secondary loops of the SWHS. This leads to an accumulative energy gain of 15.56 MJ which is a 7.82% increase in energy gain when compared to the second highest accumulative energy gain obtained using the bang–bang control strategy. The results in this table also show that with the flow rates of the proposed solution, the gain of the heat exchanger over the optimization interval is 51.64 KW which is less than those obtained with the other two strategies. Finally, it is noted that the optimal switching strategy produces the least tank and connecting pipe thermal losses.

Table 6 shows the overall impact of the pipe thermal losses on the energy collected. From this table it can be seen that pipe thermal losses range from 5.54% to 7.34% of the total energy from the collector system for each control strategy. It is important to note that insulation also plays an important role in the overall thermal losses of any system.

5.2.4. Benefits and drawbacks of the different control strategies

Each control strategy presented in this section has its benefits as well as drawbacks. In the case of bang–bang control, the control action is generally two switches during a 24 h period. The benefit to this is that no other control device is required to control the on and off switching. The drawback to using this strategy is that during its on cycle, fluid is pumped at the maximum possible flow rate, and though this increases the collector gain, it also increases the SC, tank, and connecting pipe thermal losses, thereby reducing the overall gain of the system. The optimal switching strategy on the other hand results in a reduction of SC, tank, and connecting pipe thermal losses due to the continuous on and off switching of the pump during when solar radiation is available. However, this switching also reduces the collector gain during this period. Another drawback to this control strategy is that the continuous on and off switching has a negative long term damaging effect on pump. When considering the proposed mass flow rates, though the overall system gain is increased, it should be noted that in order to obtain the varying mass flow rates, a variable flow control device such as a variable speed drive (VSD) would be required in order to control the speed of the fan. This would increase overall system cost.

6. Conclusion

The growing popularity of SWHS as an alternative to geysers connected to the grid has led to a search for methods to improve the performance of SWHS whilst meeting user power demands. Pump flow rate optimization is one such method. This paper furthers studies that are done on flow rate optimization of SWHS with specific focus placed on pump flow rate optimization of forced circulation solar water heating systems. The system considered consists of an array of six solar collectors, two storage tanks and connecting pipes. An optimization model is developed in order to determine the optimal flow rates that will maximize energy gain in the primary loop whilst meeting user defined tank temperatures with minimum energy usage in the secondary loop of the system. The model is solved using the fmincon solver in the MATLAB optimization toolbox and the results are compared to other control strategies that are commonly used in practice. These results show a 7.82% increase in the amount of energy extracted when compared to the most suitable energy efficient control strategy. The results also show system thermal losses that range between 5.54% and 7.34% for the different control strategies due to pipe losses. These results illustrate the significance and impact of mass flow rates on the system performance, overall energy gain and usage as well as on the system thermal losses. The results of this study serve a foundation for future research that could include: feasibility studies on the cost viability of the proposed system (with the pump costs included) when compared to systems with a constant flow rate or thermosyphon systems with emphasis on the payback period in order to determine the most cost effective system.

Table 6
Pipe thermal loss impact.

Control strategy	Bang–bang	Opt-switching	Proposed solution
Thermal loss impact (%)	6.03	7.34	5.54

Acknowledgement

This work is supported by the Centre for New Energy Systems (CNES) and the National Hub for the Postgraduate Programme in Energy Efficiency and Demand Side Management at the University of Pretoria.

Appendix A

This section presents the equations used to determine the solar collector parameters used in the developed model.

Transmittance absorbance factor

In order to determine the transmittance absorbance factor ($\tau\alpha$), Snell's law is first used to determine the reflected angle (θ_2) with the incidence angle (θ_1), and the indices of reflection n_1 and n_2 known. Snell's equation is shown below:

$$\frac{\sin(\theta_2)}{\sin(\theta_1)} = \frac{n_1}{n_2}, \tag{53}$$

where the perpendicular and parallel components of the reflectance are then determined using the following equations:

$$r_{(\perp)} = \frac{\sin^2(\theta_2 - \theta_1)}{\sin^2(\theta_2 + \theta_1)}, \tag{54}$$

$$r_{(\parallel)} = \frac{\tan^2(\theta_2 - \theta_1)}{\tan^2(\theta_2 + \theta_1)}. \tag{55}$$

The overall reflectance for a non-zero incidence angle and a zero incidence angle are given by:

$$r = \frac{r_{(\parallel)} + r_{(\perp)}}{2} \quad 0 < \theta_1 \leq 90, \tag{56}$$

$$r = \left(\frac{n-1}{n+1}\right)^2 \quad \theta_1 = 0. \tag{57}$$

The perpendicular component of the transmittance is given by:

$$\tau_{(\perp)} = \frac{1 - r_{(\perp)}}{1 + r_{(\perp)}}. \tag{58}$$

The transmittances due to reflectance and absorption are determined using the following equations:

$$\tau_{rn}(\theta) = 0.5\left(\frac{1-r_{(\|)}}{1+(2n-1)\cdot r_{(\perp)}} + \frac{1-r_{(\perp)}}{1+(2n-1)\cdot r_{(\perp)}}\right), \tag{59}$$

$$\tau_a = exp\left(\frac{-K\cdot L}{\cos(\theta_2)}\right). \tag{60}$$

The overall transmittance and absorbance factors are then given by:

$$\tau = t_a \cdot t_{rn}, \tag{61}$$

$$\alpha = 1 - \tau_a. \tag{62}$$

Overall thermal loss coefficient

The overall Thermal loss coefficient over the collector is given by (7), where U_t, U_b and U_e are top, bottom and edge loss coefficients. The bottom loss coefficient is given by:

$$U_b = \frac{kb}{lb}, \tag{63}$$

where *kb* and *lb* are the collector bottom thermal insulation thickness and thermal conductivity shown in Table 2. The edge loss coefficient is given by:

$$U_e = \frac{UA_{edge}}{A_c}, \tag{64}$$

where UA_{edge} and A_c are the edge loss coefficient area product and the area of the collector. The top loss coefficient is determined using the following equation:

$$U_t = \left(\frac{N}{\frac{C}{T_{pm}}\cdot\left[\frac{T_{pm}-T_a}{N+f}\right]^e} + \frac{1}{h_w}\right)^{-1} + \frac{\sigma(T_{pm}+T_a)\left(T_{pm}^2+T_a^2\right)}{\frac{1}{\varepsilon_p+0.0059Nh_w} + \frac{2N+f-1+0.133\varepsilon_p}{\varepsilon_g} - N}, \tag{65}$$

where N is the number of glass covers of the collector, ε_p and ε_g are the glass and plate emittance, T_{pm} and T_a are the mean plate and ambient temperatures, and h_w represents the wind heat transfer coefficient. T_{pm}, f,e and C are determined using the following equations:

$$T_{pm} = T_{Fi} + \frac{Q_i n/A_{coll}}{F_r U_L}\left(1 - F_{2\_prime}\right), \tag{66}$$

$$F_{2\_prime} = \frac{F_r}{F_{prime}}, \tag{67}$$

$$f = (1 - 0.09h_w - 0.1166h_w\varepsilon_p)(1 + 0.07866N), \tag{68}$$

$$e = 0.430\cdot\left(1 - \frac{100}{T_{pm}}\right), \tag{69}$$

$$C = 520\left(1 - 0.00005\cdot\beta^2\right), \tag{70}$$

where T_{fi} is the initial fluid temperature, β represents the collector tilt in degrees. For eq. (70), $0^\circ \le \beta \le 70^\circ$ otherwise $\beta = 90^\circ$ should be used.

Collector heat removal factor

When considering a standard solar collector, the fin efficiency is determined using the following equations:

$$F = \frac{m(W-D)^{-1}}{2}\cdot\tan\left[\frac{m(W-D)}{2}\right], \tag{71}$$

where

$$m = \sqrt{\frac{U_L}{k_p\delta_p}}. \tag{72}$$

In the above equations, D and W represent the collector tube external diameter and the distance between two neighbouring tubes, while k_p and δ_p represent the collector plate thickness and thermal conductivity. The collector efficiency is determined using the following equations:

$$F_{prime} = \frac{1/U_L}{w\left[\frac{1}{U_L[D+(W-D)F]} + \frac{1}{C_b} + \frac{1}{\pi D_i h_{fi}}\right]}, \tag{73}$$

$$D_i = D - 2\delta_p, \tag{74}$$

$$h_f = \left(1430 + 23.3t - 0.048t^2\right)w_{water}^{0.8}D_i^{-0.2}, \tag{75}$$

where C_b and D_i are the bond conductance and collector tube inner diameter, and h_f is the heat transfer coefficient between the circulation fluid and the tube walls. With ρ_1 representing the fluid mass density, the fluid speed is given by:

$$w_{water} = \frac{\dot{m}_1}{AW}\left[\frac{4}{\rho_1\pi D_i^2}\right], \tag{76}$$

while the average working fluid temperature t inside the tube is given by:

$$t = T_{fm} - 273.15, \tag{77}$$

with

$$T_{fm} = \frac{T_{f,in} + T_{F,out}}{2}. \tag{78}$$

Finally, the collector heat removal factor can then be evaluated using (6).

Appendix B

This section presents the equations used to determine the heat exchanger parameters used in the developed model. The heat transfer coefficients h_0 and h_1 are used to determined the rate of energy from the heat exchanger. These parameters are determined using the following equations:

$$Nu = 0.021 Re^{0.8} \cdot P_{rf}^{0.45}, \tag{79}$$

$$Nu = \frac{h_{fp} \cdot D_{serp}}{\lambda}, \tag{80}$$

$$Re = \frac{w \cdot D_{serp}}{\nu}, \tag{81}$$

$$Pr = \frac{c_p \cdot \rho \nu}{\lambda}. \tag{82}$$

In these equations, Nu, Re and Pr are the Nusselt, Reynolds and Prandtl numbers. λ, ν, c_p, and ρ represent the fluids thermal conductivity, kinematic viscosity, specific heat and mass density. These parameters above are to determine the forced convection heat loss coefficient h_{fp}. The following equations are then used to determine the natural convection heat transfer coefficient h_{pw} between the wall pipe and the circulation fluid or water that is in the storage tank:

$$Nu = \frac{h_{pw}(D_{serp} + 2w_{serp})}{\lambda}, \tag{83}$$

$$Nu = 0.5\left(G_{rf} \cdot P_{rf}\right)^{0.25} \left(\frac{P_{rf}}{P_{rp}}\right)^{(0.25)} \quad 10^3 \le (G_{rf} \cdot P_{rf}) \le 10^8, \tag{84}$$

$$Gr = g\frac{h_{pw}(D_{serp} + w_{serp})^3 \beta (T - T_s)}{\nu^2}, \tag{85}$$

where g, β represent the gravitational acceleration and the thermal expansion coefficient. T and T_s represent the average and tank temperature for the circulation fluid and water. D_{serp} and w_{serp} represent the serpentine diameter and circulation fluid/water speed through the serpentine. The average linear heat transfer coefficient is then determined using the following relation:

$$\frac{1}{h_{lin}} = \frac{1}{\pi D_{serp} \cdot h_{fp}} + \frac{1}{2\pi \cdot \lambda_{serp}} \times \ln\frac{D_{serp} + 2w_{serp}}{2\pi \cdot D_{serp}} + \ln\frac{D_{serp} + 2w_{serp}}{\pi \cdot h_{pw}(D_{serp} + 2w_{serp})}, \tag{86}$$

where λ_{serp} is the thermal conductivity of the serpentine's material. The heat transfer coefficients h_0 and h_1 are determined using (19).

Appendix C

This section presents the equations used to determine the parameters of the pumps used in the developed model.

Computation of pump power

The computation of the pump mechanical power required to circulate the fluid in the primary and secondary loops of the system is obtained using (21)–(37).

Computation of the pressure loss coefficients

The pressure loss coefficient δ_{coll} is calculated using:

$$\delta_{coll} = \frac{1}{0.788B_3 + 0.029K + \frac{0.115a_{coll}}{\dot{a}_{coll}} - \frac{0.115a_{coll}}{\dot{a}_{coll}} - 0.090}, \tag{87}$$

where a_{coll} and $\dot{a}_{coll}$ are the inlet and outlet cross sectional areas of the drums at the inlet and outlet of the solar collector. Factors K and B are determined using the following equations:

$$K = 1 - \frac{a_f}{a_{coll}}, \tag{88}$$

$$B_3 = \frac{\overline{a}}{\sqrt{0.6 + \left(\frac{a_p}{a_p^{\cdot}}\right)^2 + \delta_{dev} + \delta_p}}, \tag{89}$$

where a_p and $\dot{a}_p$ are the inlet and outlet cross sectional areas of the pipes at the inlet and outlet of the solar collector. These parameters are taken to be identical for solar collector used. The parameter δ_{dev} refers to the pressure losses in devices placed along the length of the pipe. Parameter $\overline{a}$ is obtained using:

$$\overline{a} \equiv \frac{na_p}{a_{coll}}, \tag{90}$$

where n is the number of pipes in the solar collector. The linear pressure loss coefficient is given by:

$$\delta_p \equiv \lambda_p \frac{l_{pipe}}{d_{pipe}}, \tag{91}$$

where λ_p is the friction factor of the pipe. The friction factor is calculated using the following equation:

$$\lambda = \begin{cases} 0.3164 Re^{-0.25} & \text{if } 3^3 \le Re \le 10^5, \\ 0.0054 + 0.3964 Re^{-0.3} & \text{if } 10^5 \le Re \le 2 \times 10^6, \\ 0.0032 + 0.221 Re^{-0.3} & \text{if } Re \ge 2 \times 10^6. \end{cases} \tag{92}$$

Reynolds number Re is determined using:

$$Re = \frac{wd}{\nu}, \tag{93}$$

where w is the fluid speed at the duct, d is the diameter of the duct and v is the kinematic viscosity of the fluid.

References

[1] Y. Guo, M. Pan, Y. Fang, Optimal power management of residential customers in the smart grid, Parallel Distrib. Syst. IEEE Trans. 23 (9) (2012) 1593–1606.

[2] A. Barbato, A. Capone, G. Carello, M. Delfanti, M. Merlo, A. Zaminga, Cooperative and non-cooperative house energy optimization in a smart grid perspective, in: World of Wireless, Mobile and Multimedia Networks (WoWMoM), 2011 IEEE International Symposium on a, 2011, pp. 1–6.

[3] M. Pedrasa, T. Spooner, I. MacGill, Coordinated scheduling of residential distributed energy resources to optimize smart home energy services, Smart Grid IEEE Trans. 1 (2) (2010) 134–143.

[4] F. Aghbalou, F. Badia, J. Illa, Exergetic optimization of solar collector and thermal energy storage system, Int. J. Heat Mass Transf. 49 (78) (2006) 1255–1263.

[5] J. Duffie, W. Beckman, Solar Engineering of Thermal Processes, third ed., Wiley, 2006.

[6] Y.W. Wong, K. Sumathy, Thermodynamic analysis and optimization of a solar thermal water pump, Appl. Therm. Eng. 21 (5) (2001) 613–627.

[7] V. Badescu, Optimal control of flow in solar collector systems with fully mixed water storage tanks, Energy Convers. Manag. 49 (2) (2008) 169–184.

[8] V. Badescu, Optimal control of flow in solar collectors for maximum exergy extraction, Int. J. Heat Mass Transf. 50 (2122) (2007) 4311–4322.

[9] J. Vargas, J. Ordonez, E. Dilay, J. Parise, Modeling, simulation and optimization of a solar collector driven water heating and absorption cooling plant, Sol. Energy 83 (8) (2009) 1232–1244.

[10] M. Kovarik, P. Lesse, Optimal control of flow in low temperature solar heat collector, Sol. Energy 18 (5) (1976) 431–435.

[11] A. Orbach, C. Rorres, R. Fischl, Optimal control of a solar collector loop using a distributed-lumped model, Automatica 17 (3) (1981) 535–539.

[12] R. Kicsiny, Performance modelling of combined solar heating systems with ordinary- and with an energetically-based control, in: Energy and

Environment in the Practice, Proc Seminar of Doctorate Students from Justus Liebig University (Giessen) and Szent Istvan University,Godollo, August 19–21, 2008, pp. 67–78.
[13] R. Kicsiny, I. Farkas, Improved differential control for solar heating systems, Sol. Energy 86 (11) (2012) 3489–3498.
[14] S. Farahat, F. Sarhaddi, H. Ajam, Exergetic optimization of flat plate solar collectors, Renew. Energy 34 (4) (2009) 1169–1174.
[15] R. Kicsiny, J. Nagy, C. Szalki, Extended ordinary differential equation models for solar heating systems with pipes, Appl. Energy 129 (0) (2014) 166–176.
[16] J. Smith, H. Van Ness, M. Abbott, Introduction to Chemical Engineering Thermodynamics, international ed., McGraw Hill, 2005.
[17] Z. Morvay, D. Gvozdenac, Applied Industrial Energy and Environmental Management, international ed., John Wiley & Sons, 2009.
[18] M.A. Stubblefield, S.S. Pang, V.A. Cundy, Heat loss in insulated pipe the influence of thermal contact resistance: a case study, Compos. Part B Eng. 27 (1) (1996) 85–93.
[19] A.D. Rosa, H. Li, S. Svendsen, Method for optimal design of pipes for low-energy district heating, with focus on heat losses, Energy 36 (5) (2011) 2407–2418.
[20] A.A.M. Sayigh, Solar Thermal Engineering, illustrated ed., Acedemic Press, 1977.
[21] J.R. Howel, Solar-Thermal Energy Systems, McGraw-Hill, 1982.
[22] A.A. Badran, M.F. Mustafa, W.K. Dawood, Z.K. Ghazzawi, On the measurement of bond conductance in solar collector absorber plate, Energy Convers. Manag. 49 (11) (2008) 3305–3310. Special Issue 3rd International Conference on Thermal Engineering: Theory and Applications.
[23] C.C. Smith, T.A. Weiss, Design application of the Hottel-Whillier-Bliss equation, Sol. Energy 19 (2) (1977) 109–113.
[24] S.A. Kalogirou, Chapter 5-solar water-heating systems, in: S.A. Kalogirou (Ed.), Solar Energy Engineering, second ed., Academic Press, Boston, 2014, pp. 257–321.
[25] P.A. Stark, Introduction to Numerical Methods, Celtis Publisher, 1970.
[26] A. Lauschagne, A. van der Merwe, N. van Rensburg, L. Zietsman, An Introduction to Numerical Analysis, seventh ed., Celtis Publisher, 2014.
[27] M. Dehghandokht, M.G. Khan, A. Fartaj, S. Sanaye, Flow and heat transfer characteristics of water and ethylene glycolwater in a multi-port serpentine meso-channel heat exchanger, Int. J. Therm. Sci. 50 (8) (2011) 1615–1627.
[28] M. Dehghandokht, M.G. Khan, A. Fartaj, S. Sanaye, Numerical study of fluid flow and heat transfer in a multi-port serpentine meso-channel heat exchanger, Appl. Therm. Eng. 31 (10) (2011) 1588–1599.
[29] W. Durfee, Z. Sun, Fluid Power Syatem Dynamics, @ONLINE, 2009. URL, http:www.me.umn.edu/wkdurfee/projects/ccefp/fp-chapter/fluid-pwr.pdf.
[30] H. Zhang, X. Xia, J. Zhang, Optimal sizing and operation of pumping systems to achieve energy efficiency and load shifting, Electr. Power Syst. Res. 86 (0) (2012) 41–50.
[31] @ONLINE, Duratherm Extended Life Fluids, 2015. URL, https//durathermfluids.com/pdf/productdata/heattransfer/duratherm-600.pdf.
[32] C. Lopez, Matlab Optimization Techniques, Springer, 2014.
[33] F. Hilmer, K. Vajen, A. Ratka, H. Ackermann, W. Fuhs, O. Melsheimer, Numerical solution and validation of a dynamic model of solar collectors working with varying fluid flow rate, Sol. Energy 65 (5) (1999) 305–321.